The Nanomechanical Properties of Lipid Membranes are Significantly Influenced by the Presence of Ethanol

Frank W. S. Stetter and Thorsten Hugel*
IMETUM, Physik-Department, E22a, Technische Universität München, Munich, Germany

ABSTRACT Ethanol has a profound impact on biological systems and is moreover used in various medical and nonmedical applications. Its interaction with the lipid part of biological membranes has been the subject of intensive studies, but surprisingly, to our knowledge, no study has examined the influence of ethanol on lipid bilayer nanomechanics. We performed atomic force microscopy-based measurements to assess the influence of ethanol on the nanomechanical properties of fluid supported lipid bilayers. Ethanol significantly reduces membrane stability, bilayer thickness, Young's modulus, area stretch modulus, and bending stiffness. Altogether, our data suggest that ethanol addition to supported lipid bilayers supports both the hydrophobic and the hydrophilic permeation pathways by a decrease of bilayer thickness and reduced stability, respectively.

INTRODUCTION

The interaction of ethanol and other small amphiphilic molecules with biological membranes has numerous aspects. For example, high concentrations of ethanol up to 60% have been used in transdermal drug delivery to enhance the permeation of drugs for many years despite the lack of detailed knowledge about its mode of action (1). In addition, the interaction of ethanol with lipid membranes is relevant in the production of alcoholic beverages where yeast cell membranes have to withstand ethanol concentrations of >10%. Finally, its effect on lipid bilayers is discussed in the context of general anesthesia, where local concentrations are not known (2–4). When interacting with lipid bilayers, ethanol and other short-chain alcohols seem to be mainly located in the headgroup region where hydrogen bonds between the alcohols and the phosphate and carbonyl groups of the lipids can form (5,6). This changes the packing in the lipid membrane and might cause previously observed effects on bilayer properties like an increase in elasticity, fluidity, and permeability upon the addition of alcohol (7–9). Such modifications in bilayer mechanics can change the shape and stability of cells and liposomes, and impede membrane protein function (10,11). Surprisingly, even though there is a huge number of reports that describe the physiological and biochemical effects of ethanol, experimental studies investigating the impact of ethanol on lipid membrane mechanics are very rare.

Supported lipid bilayers (SLBs) are routinely used for lipid membrane studies (12). They can be considered as a first approximation of the lipid part of cellular membranes. SLBs opened the road for the investigation of lipid membranes with sophisticated surface-sensitive techniques like surface plasmon resonance (13), total internal reflection fluorescence microscopy (14), the surface force apparatus (15), and atomic force microscopy (AFM) (14,16,17). In particular, AFM turned out to be a valuable imaging technique to study SLBs because it provides molecular spatial resolution in all three dimensions and can be operated in physiological environments (18). A natural extension of these methods is to probe the mechanics of lipid bilayers by first elastically deforming and then puncturing the SLB by a vertically moving AFM tip (see Fig. 1) (19). This method has shown that bilayer composition, buffer composition, ionic concentration, and the temperature are important factors determining bilayer mechanics (19–23).

We present AFM nanomechanical measurements of the influence of ethanol on five parameters characterizing supported lipid bilayer nanomechanics, namely puncture force, thickness of the bilayer, Young's modulus, area stretch modulus, and bending stiffness. This complements previous mechanical measurements employing the micropipette aspiration technique on whole vesicles (9,24) and allows, to our knowledge for the first time, to quantify the effect of ethanol on any of these mechanical properties for SLBs and on the nanoscale.

MATERIALS AND METHODS

DOPC (1,2-dioleoyl-*sn*-glycero-3-phosphocholine) and Rhodamine-PE (1,2-dioleoyl-*sn*-glycero-3-phosphoethanolamine-N-(lissamine rhodamine B sulfonyl)) were purchased from Avanti Polar Lipids (Alabaster, AL). HPLC water and Hepes were purchased from Biochrom (Berlin, Germany). Ethanol (pure) was obtained from Merck (Darmstadt, Germany). Chloroform (HPLC-grade) was purchased from Sigma-Aldrich (St. Louis, MO).

Preparation of unilamellar vesicles

DOPC was dissolved in chloroform to a final concentration of 1 mg/mL with Rhodamine-PE as a fluorescent marker. The concentration of the fluorescent marker was as low as 0.1% (mol) to guarantee that the dye does not influence the mechanical properties of the lipid bilayer (which happens only at concentrations of around 10%). The solution was filled in a glass vial and

Submitted September 28, 2012, and accepted for publication January 14, 2013.

*Correspondence: thorsten.hugel@ph.tum.de

Editor: Simon Scheuring.

0006-3495/13/03/1049/7 $2.00

http://dx.doi.org/10.1016/j.bpj.2013.01.021

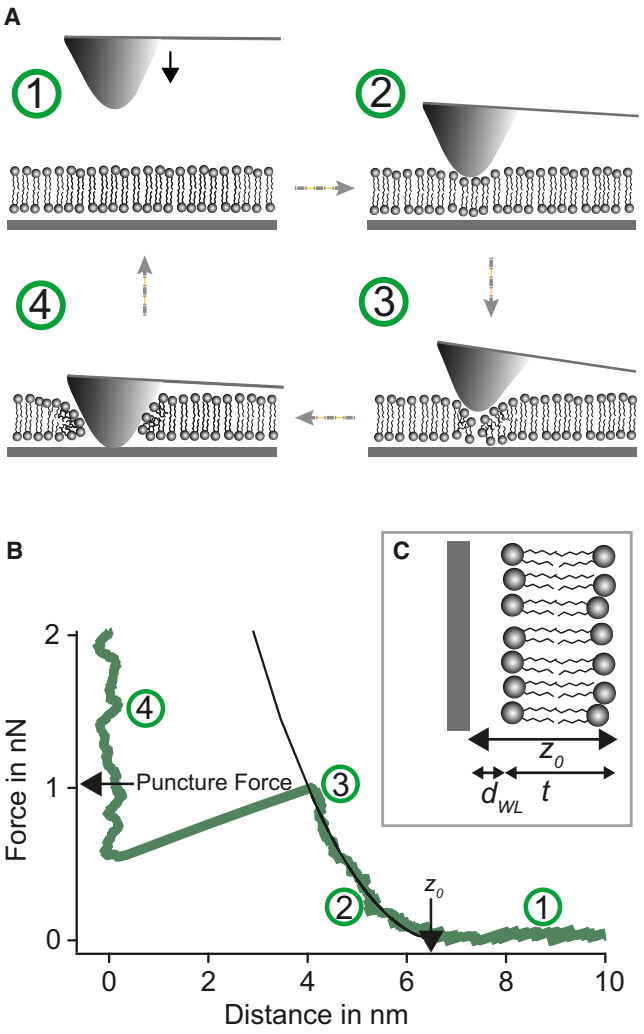

FIGURE 1 (*A*) Four-step illustration of a puncture curve on a SLB. The tip is approached toward the SLB (**1** → **2**) and starts to bend upward as soon as it interacts with the SLB (**2** → **3**). At some point the SLB fails and the tip breaks through contacting the supporting mica surface (**3** → **4**). The tip is then retracted for the next puncture curve (**4** → **1**). (*B*) Typical puncture curve with modified Hertz model fitted to the regime of elastic deformation (see main text for details of the fit). (*C*) There is good evidence that a water layer of ~1 nm exists in between the bilayer and the substrate ($d_{WL} = 1$ nm). This has to be considered in determining the bilayer thickness t.

chloroform was evaporated by a nitrogen flow followed by vacuum evaporation for at least 6 h at 0.1 mbar to ensure the absence of chloroform traces. 1 mL of an aqueous buffer (10 mM Hepes, 4 mM $CaCl_2$) was then added, and after gently shaking for 30 min multilamellar vesicles were obtained. To form unilamellar vesicles, the solution was extruded (Mini-Extruder, Avanti Polar Lipids) 31 times using a 100 nm filter (Nuclepore, Whatman, Piscataway, NJ) and allowed to equilibrate over night at 4°C.

Preparation of supported lipid bilayers

SLBs were formed on mica via the vesicle fusion method (25). As model lipid we chose DOPC, which has a main transition temperature of −20°C and was therefore in the liquid-disordered state at the temperatures used for the experiments (30°C). To form a supported lipid bilayer the vesicles have to fuse with the surface of a freshly cleaved mica plate (1 cm^2) that was glued into a temperature controllable fluid cell. To that aim, the vesicle solution was diluted 1 to 10 using the same buffer as before. 50 μL were then applied to the mica sheet for an incubation time of 45 min. Afterward the fluid cell was gently rinsed with 200 mL of water and incubated at 50°C for 30 min. After that, the fluid cell was allowed to slowly cool down to room temperature and rinsed again with at least 200 mL of pure water. Finally, the quality of the bilayer was optically checked with fluorescent microscopy. If the density distribution of the fluorophores was not uniform, or if too many nonfused vesicles were present, the sample was discarded.

AFM imaging and force spectroscopy

AFM imaging and force spectroscopy were performed using an MFP-3D AFM (Asylum Research, Santa Barbara, CA). Triangular silicon nitride cantilevers (DNP-S, Bruker, Santa Barbara, CA) with a nominal tip radius of 10 nm were used for both imaging and force spectroscopy. Nominal spring constants were between 0.1 and 0.3 nN/nm and were determined by applying the thermal noise method (26,27). Imaging was performed in intermittent contact mode, before and after performing force measurements, to make sure that puncturing had not irreversibly damaged the bilayer membrane (Fig. 2, *A* and *B*).

Each data point consisted of 200–400 puncture curves that were taken in a raster mode fashion over an area of 3 × 3 μm^2 (force map). Puncture measurements were performed by vertically approaching the AFM tip toward the SLB (Fig. 1 *A*, **1** → **2**). When the tip is close to the bilayer, it starts to interact with the surface resulting in a bending upward (Fig. 1 *A*, **2** → **3**). At low forces this interaction is mainly due to Derjaguin, Landau, Verwey, and Overbeek and hydration forces. As the force rises the bilayer is compressed by steric interaction between the tip and the membrane until it yields (Fig. 1 *A*, **3** → **4**). The tip then jumps to the supporting surface. For the next puncture curve the tip was retracted by ~500 nm (Fig. 1 *A*, **4** → **1**), moved vertically to the next raster point, and approached again to the bilayer. The tip was moved with a vertical velocity of 500 nm/s.

Data evaluation

Typically, all analysis steps were carried out automatically by a homewritten algorithm based on the software IGOR Pro 6 (WaveMetrics, Portland, OR).

Puncture curves were first recorded as cantilever deflection versus piezo extension. The cantilever sensitivity was then determined for each individual curve by measuring the slope of the deflection-extension curve after the breakthrough, i.e., when the tip had contact with the hard mica surface. Together with the spring constant (see above) this allowed us to calculate force versus distance curves.

As puncture force we took the maximal force before the breakthrough. After SLB formation, a layer of a few water molecules exists between

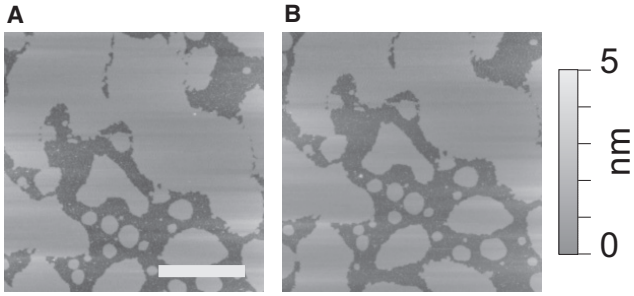

FIGURE 2 AFM images of lipid membrane patches in 20% ethanol. The figure shows AFM images before (*A*) and after (*B*) force curves were taken in the depicted area. Imaging was accomplished in intermittent mode and was used to verify that the puncture curves had not damaged lipid bilayer integrity. The scale bar is 1 μm.

the support and the lipid heads. This layer can be assumed to be roughly 1 nm thick (12,28–30) and is likely stabilized by the hydrophilic mica and the lipid surface. Unfortunately, for water/ethanol mixtures it is not clear if such a layer exists. Therefore, in the following, we differentiated two cases when ethanol was present: one where we assume a water/ethanol layer of 1 nm between mica and the lipid bilayer (case 1) and, one case where the water/ethanol layer does not exist (case 0). For the modeling of the puncture curves in pure water, we always assumed a water layer of 1 nm. To extract further mechanical information from the puncture curves, we used a modified Hertz-model (31)

$$F = \frac{16\,Y}{9} R^{\frac{1}{2}} (z - z_0)^{\frac{3}{2}} \left[1 + 0.884\chi + 0.781\chi^2 + 0.386\chi^3 + 0.0048\chi^4\right], \quad (1)$$

with $\chi = (R \times (z - z_0))^{1/2}/t$. This model includes semiempirical corrections for the finite thickness of the bilayer in contrast to an infinite half-space, which is assumed in the original Hertz model (32). Fit parameters are the Young's modulus Y and the point z_0 where the fit reaches 0 nN (Fig. 1 *B*). The bilayer thickness t can be obtained by subtracting the thickness of the water layer d_{WL} between the supporting surface (which is located at $z = 0$ nm) and the bilayer from the onset of the elastic deformation z_0 as obtained from the fit (Fig. 1 *C*), i.e., $t = z_0 - d_{WL}$. Assuming a water/ethanol layer implies that the layer is compressed simultaneously with the bilayer. Because both the mica and the proximal surface of the lipid bilayer constitute highly hydrophilic surfaces we assume that the layer is stabilized between the two surfaces. We further assume that this stabilization is strong enough to result in a Young's Modulus much larger than one of the lipid bilayer. We therefore neglect this layer to determine the bilayer's Young's Modulus resulting in a lower limit. We then fit the modified Hertz-model to the elastic part of the puncture curves starting from 0.1 nN (where we expect the Derjaguin, Landau, Verwey, and Overbeek and hydration forces to be sufficiently small) (22,33) up to the point where the bilayer yields.

The Young's modulus Y and bilayer thickness t are used to calculate the area stretch modulus k_A and the bending stiffness k_c by applying thin shell theory (34–36),

$$k_A = \frac{Yt}{(1 - \nu^2)}, \quad (2)$$

$$\kappa_C = \frac{Yt^3}{24(1 - \nu^2)}, \quad (3)$$

assuming a Poisson ratio ν of 0.5.

RESULTS

First, we evaluate the puncture force, which is defined as the maximal vertical force a bilayer can withstand before failing upon vertical compression. It is therefore a measure of in-plane lipid cohesion or stated another way, a measure for bilayer stability. It depends on a great variety of physical (e.g., temperature, lipid chain saturation, and electrolyte concentration) and experimental (e.g., tip radius and tip chemistry) parameters, therefore, the experiments were carried out using the same tip for a complete set of concentrations. In addition, we used one and the same cantilever velocity (500 nm/s) for the presented experiments because the puncture force (but not the other elastic parameters) depends on velocity (see the Supporting Material Fig. S1). At the end of a set of ethanol concentrations (~3000 puncture curves) we returned to 0% ethanol and measured the same force as before showing that the tip radius had not changed. However, membranes are apparently rendered more susceptible to mechanical distortion (like exchange of liquid or tip sample interaction) upon ethanol addition. Therefore, more than half of our experiments were terminated after the addition of 40% ethanol. We have performed this type of measurements more than 10 times with more than five different AFM tips. The results of the best AFM tip are summarized in Table 1. Presented in Fig. 3 *A* are the average puncture forces obtained for different ethanol concentrations. Each data point is based on 200–400 puncture curves. The forces decrease almost linearly with ethanol concentration from 1.0 nN in pure water to 0.3 nN in 40% ethanol solution, constituting a significant reduction in bilayer stability. Fig. 3 *B* shows the decrease in bilayer thickness from the puncture measurements for the different ethanol concentrations. The bilayer thickness already depends on the model assumptions used, in particular, if there is a water/ethanol layer of 1 nm in between the bilayer and the substrate (case 1) or if there is none (case 0)—see Methods section for details. We find a reduction in lipid bilayer thickness of 1.9 nm (from 5.7 to 3.9 nm) when the ethanol concentration is increased from 0% to 40% in case 0 (spheres) and a reduction of 2.8 nm (from 5.7 to 2.9 nm) in case 1. The decrease is again linear when no water/ethanol layer is assumed (case 0) and nonlinear if such a layer of 1 nm thickness (like for pure water) is assumed (case 1). Fig. 3 *C* shows that upon ethanol addition the Young's modulus is reduced. For case 0 the decrease is linear resulting in a reduction from 15.2 to 5.5 MPa for the addition of 40% ethanol. For case 1, i.e., where the bilayer is

TABLE 1 Effect of different ethanol concentrations on lipid membrane mechanical parameters

Concentration (vol:vol)	Puncture force (nN)	Bilayer thickness (nm)		Young's modulus (MPa)		Area stretch modulus (mN/m)		Bending stiffness (10^{-19}J)	
		Case 1	Case 0	Case 1	Case 0	Case 1	Case 0	Case 1	Case 0
0%	1.00 ± 0.17	5.7 ± 0.5		15.2 ± 4.0		116 ± 35		1.56 ± 0.23	
10%	0.91 ± 0.17	3.9 ± 0.7	4.7 ± 0.7	8.1 ± 2.2	12.2 ± 3.5	43 ± 10	78 ± 18	0.29 ± 0.08	0.76 ± 0.18
20%	0.74 ± 0.20	3.6 ± 0.8	4.3 ± 0.7	7.3 ± 2.3	11.0 ± 1.3	28 ± 17	68 ± 10	0.18 ± 0.08	0.55 ± 0.21
40%	0.31 ± 0.13	2.9 ± 0.8	3.8 ± 0.5	2.7 ± 1.6	5.5 ± 2.7	13 ± 5	30 ± 10	0.06 ± 0.03	0.20 ± 0.07

See main text for details.

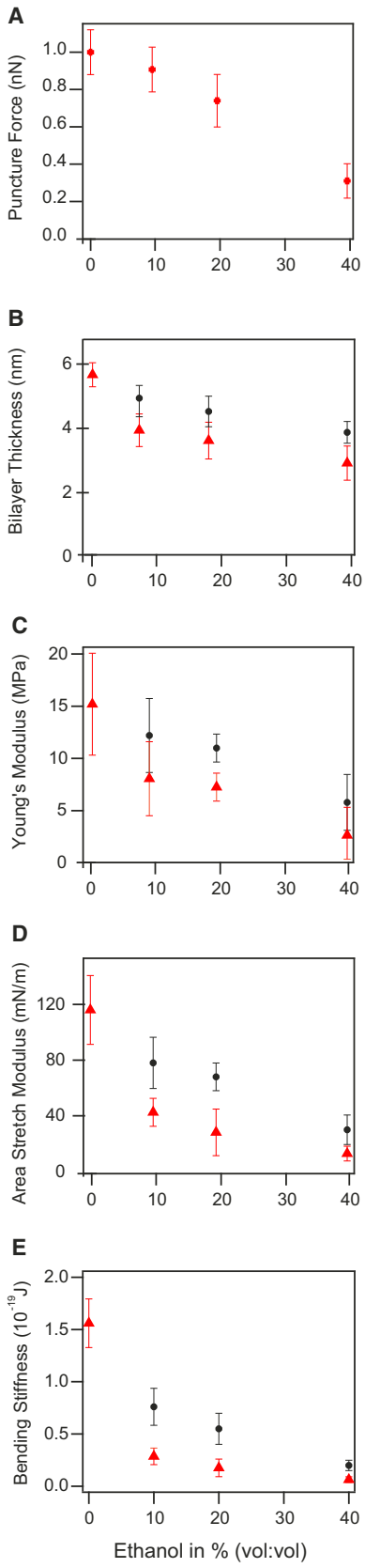

FIGURE 3 Lipid bilayer parameters obtained from the puncture curves. (*A*) Puncture force, (*B*) bilayer thickness, (*C*) Young's modulus, (*D*) area stretch modulus, and (*E*) bending stiffness. Each data point is based on 200 to 400 puncture curves. Triangles show the results assuming a water/ethanol layer between the mica support and the lipid bilayer (as for *pure water*, case 1). Circles show case 0 in which no such layer is assumed (which is more likely as detailed in the main text). Data points represent the mean values of the Gaussian fits to the data. Error bars are ± standard deviation.

assumed to be thinner, the values are decreasing in a nonlinear fashion and faster than in case 0. This is a direct consequence of the model because t enters the model nonlinearly. Based on the bilayer thickness and the Young's modulus (which is directly derived from the modified Hertz model), we calculated the area stretch modulus k_A and the bending stiffness k_c to compare our measurement with other studies where area stretch moduli and bending stiffnesses were investigated. To this end, we applied thin shell theory (Eq. 2 and Eq. 3). The Poisson ratio ν was set to 0.5 to account for incompressibility. This results in the area stretch moduli presented in Fig. 3 *D*. Starting from 116 nN/m in pure water, k_A decreases to 30 mN/m (case 0) in a linear and to 27 mN/m (case 1) in a nonlinear fashion for 40% ethanol. As can be seen from Fig. 3 *E*, k_c drops nonlinearly from 1.56×10^{-19} for pure water to 0.20×10^{-19} for 40% ethanol in case 0 and to 0.06×10^{-19} for 40% ethanol in case 1.

DISCUSSION

To the best of our knowledge, this is the first systematic study that reports on the modifications to the nanomechanical properties of supported lipid bilayers when exposed to varying ethanol concentrations. Hence, we have to compare most of our results to either studies on solid supported bilayers without ethanol, or to studies that deal with the effect of ethanol but employ other lipid models than SLBs. Because our measurements were nanoscopic, i.e., taken over an area where the important membrane processes take place (33), we were especially interested if our nanoelastic values are comparable to those obtained by mechanical measurements on the microscale (9,24,37).

The puncture forces lie in the range of forces found in other puncture experiments when done in pure water and on DOPC or DOPC-rich fluid SLBs (21). Additionally, the decreasing trend, which we observe for increasing ethanol concentrations, compares well with lysis tension measurements in micropipette aspiration experiments (9).

The observed changes in bilayer thickness t are in agreement with a reported decrease by 1.6 nm when the amount of ethanol is changed from 0% to 34% (38). In this study, AFM imaging was used to measure differences in supported lipid bilayer thickness upon ethanol addition.

In a recent study (39), the Young modulus Y of the fluid phases of DOPC/dipalmitoylphosphatidylcholine (DPPC)-SLB mixtures was found to be 19.3 MPa in very good agreement with the 15.2 MPa in our study (Fig. 3

C). However, some authors find Young's moduli of fluid SLBs, which are almost an order of magnitude higher than our values (20). The fact that in these studies a semiinfinite sample was assumed for fitting (rather than the thinness-corrected model we used for our data evaluation) seems to underscore the importance of taking the influence of the support into account. The changes in the area stretch modulus k_A and the bending stiffness k_c, as obtained by invoking thin shell theory, are a consequence of the changes in Y and t. Our value for the measurement of k_A in pure water agrees very well with the one obtained in (39) using PeakForce-AFM on SLBs. The decreasing trend of k_A and k_c values parallels the ones found in (24) obtained with the micropipette aspiration technique on vesicles, even though we measured smaller absolute values for k_A and a faster decreasing tendency for k_c. Given that our results were obtained with a completely different technique and on the nanolevel, they compare surprisingly well with measurements where these parameters were obtained on the microlevel. The nonlinear decrease of several parameters shows that already small amounts of ethanol can have a huge impact on lipid membrane elastic parameters.

Altogether, our results show that the trends and magnitudes for lipid membrane elastic parameters are comparable to those found in other studies. Our results now allow to support the following underlying molecular mechanism for ethanol-lipid bilayer interaction (Fig. 4): When ethanol is added to an aqueous solution hosting a lipid membrane, ethanol molecules adsorb to the lipid/water interface with their methyl-group directed to the hydrophobic core (5). Their surface density, for concentrations like the ones considered in this study, depends roughly linearly on the bulk concentrations (9). They displace water molecules and form hydrogen bonds with the phosphate and carbonyl groups (40). This leads to an increase in effective headgroup area (24) and, as a consequence, to a decrease in headgroup-headgroup interaction. Our observed decrease in puncture force supports such a reduction in headgroup-headgroup interaction. Because lipid bilayers can roughly be considered as incompressible, the increased effective headgroup area and thus enlarged bilayer surface, should lead to a thinning of the membrane, exactly what we measured. A further consequence of reduced headgroup-headgroup interaction is a decrease in the order parameter of the hydrocarbon chains (41), which results in a reduction of the Young's modulus—again what we observed.

To evaluate the elasticity, we chose a semiempirical model, which is presented in (31). The model is based on Hertz' theory and extended by additional terms that take thin layers into account. Even though the model is quite simple (as is the original Hertz model) and not explicitly intended to describe lipid bilayers, it works surprisingly well and gives Young's moduli, which are in good agreement with recently reported elasticity measurements on SLBs (39). There are, to the best of our knowledge, no studies that report on the thickness of the water/ethanol layer between mica and a SLB in a water/ethanol mixture. However, knowledge of this thickness is important to get a correct bilayer thickness. For this reason, we considered two cases: one in which there is a water/ethanol layer between the mica support and the lipid bilayer (case 1) and one case in which there is no such layer (case 0).

The sharp decrease in onset-distance z_0 from 0% to 10% (Fig. 5, Fig. S2) suggests that this reduction has, in addition to bilayer thinning, a second reason, which might be the removal of water layer between the lipid membrane and the support upon the addition of ethanol—favoring case 0. This is consistent with the observation that the hydration force between two silica surfaces in water is dramatically reduced when ethanol (even as low as 10%) is added to the water (42). If this effect is due to hydrogen bond breaking by ethanol, a reduction in hydration force might as well happen in our mica-DOPC system.

CONCLUSION

We have measured the effect of ethanol on several local nanomechanical properties of supported lipid bilayers. The

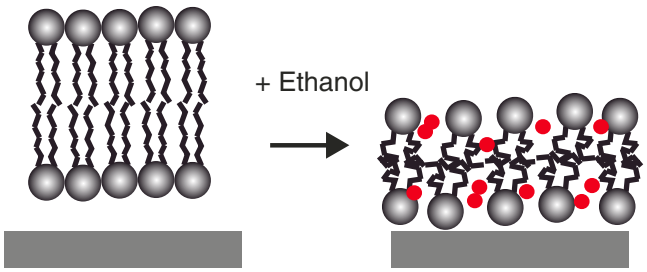

FIGURE 4 Illustration of proposed molecular mechanism for ethanol-SLB interaction. Upon ethanol (*circles*) addition, the membrane thickness is reduced with a concomitant increase in membrane area. Additionally, the order parameter of the hydrocarbon chains is reduced and the cleft between the mica support and the lower lipid headgroups disappears.

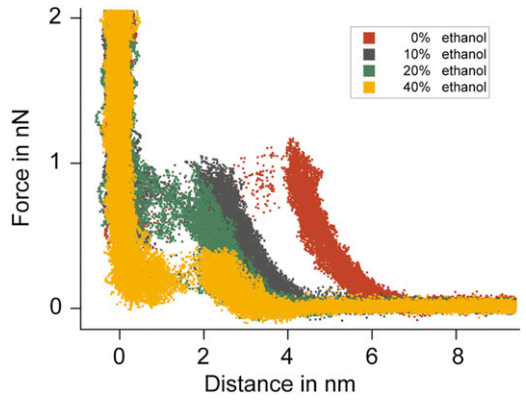

FIGURE 5 Superposition of >750 puncture curves acquired in different ethanol concentrations. Note the considerable change in onset distances when the ethanol concentration is increased from 0% to 10%, favoring case 0.

fact that both the puncture force and the bilayer thickness decrease with ethanol concentration is in line with the observation that ethanol enhances membrane permeation. Moreover, it suggests that the increased permeation is caused by both, a hydrophilic pathway (through the decrease in bilayer thickness) and a hydrophobic pathway through a reduced stability of the bilayer and therefore enhanced hydrophilic pore formation. We have further shown that the change in bilayer elastic parameters depends on the ethanol concentration and is qualitatively and quantitatively comparable to the change found on nonsupported lipid bilayers. Finally, our measurements indicate that the water layer in between the support and a lipid bilayer largely vanishes upon the addition of 10% or more ethanol.

SUPPORTING MATERIAL

Two figures and their legends are available at http://www.biophysj.org/biophysj/supplemental/S0006-3495(13)00091-X.

We thank Prof. Erich Sackmann for helpful discussions, Prof. Janshoff for help with SLB formation, the Nanosystems Initiative Munich (NIM), the Hanns-Seidel-Stiftung (HSS), and the ESF EuroMEMBRANE CRP OXPL (Hu 997/7-1) for financial support.

REFERENCES

1. Williams, A. C., and B. W. Barry. 2004. Penetration enhancers. *Adv. Drug Deliv. Rev.* 56:603–618.
2. Meyer, H. 1899. On the theory of narcosis. *Arch Exp Pathol Pharmakol.* 42:109–118.
3. Overton, E. 1901. Studien über die Narkose zugleich ein Beitrag zur allgemeinen Pharmakologie. Gustav Fischer, Jena, Germany.
4. Cantor, R. S. 1997. The lateral pressure profile in membranes: a physical mechanism of general anesthesia. *Biochemistry.* 36:2339–2344.
5. Feller, S. E., C. A. Brown, …, K. Gawrisch. 2002. Nuclear Overhauser enhancement spectroscopy cross-relaxation rates and ethanol distribution across membranes. *Biophys. J.* 82:1396–1404.
6. Rottenberg, H. 1992. Probing the interactions of alcohols with biological membranes with the fluorescent probe Prodan. *Biochemistry.* 31:9473–9481.
7. Chin, J. H., and D. B. Goldstein. 1977. Effects of low concentrations of ethanol on the fluidity of spin-labeled erythrocyte and brain membranes. *Mol. Pharmacol.* 13:435–441.
8. Komatsu, H., and S. Okada. 1997. Effects of ethanol on permeability of phosphatidylcholine/cholesterol mixed liposomal membranes. *Chem. Phys. Lipids.* 85:67–74.
9. Ly, H. V., and M. L. Longo. 2004. The influence of short-chain alcohols on interfacial tension, mechanical properties, area/molecule, and permeability of fluid lipid bilayers. *Biophys. J.* 87:1013–1033.
10. Sukharev, S. I., P. Blount, …, C. Kung. 1997. Mechanosensitive channels of *Escherichia coli:* the MscL gene, protein, and activities. *Annu. Rev. Physiol.* 59:633–657.
11. Goulian, M., O. N. Mesquita, …, A. Libchaber. 1998. Gramicidin channel kinetics under tension. *Biophys. J.* 74:328–337.
12. Sackmann, E. 1996. Supported membranes: scientific and practical applications. *Science.* 271:43–48.
13. Besenicar, M., P. Macek, …, G. Anderluh. 2006. Surface plasmon resonance in protein-membrane interactions. *Chem. Phys. Lipids.* 141:169–178.
14. Oreopoulos, J., R. F. Epand, …, C. M. Yip. 2010. Peptide-induced domain formation in supported lipid bilayers: direct evidence by combined atomic force and polarized total internal reflection fluorescence microscopy. *Biophys. J.* 98:815–823.
15. Benz, M., T. Gutsmann, …, J. Israelachvili. 2004. Correlation of AFM and SFA measurements concerning the stability of supported lipid bilayers. *Biophys. J.* 86:870–879.
16. Milhiet, P.-E., F. Gubellini, …, D. Lévy. 2006. High-resolution AFM of membrane proteins directly incorporated at high density in planar lipid bilayer. *Biophys. J.* 91:3268–3275.
17. Lorenz, B., R. Keller, …, A. Janshoff. 2010. Colloidal probe microscopy of membrane-membrane interactions: from ligand-receptor recognition to fusion events. *Biophys. Chem.* 150:54–63.
18. Müller, D. J., H. J. Sass, …, A. Engel. 1999. Surface structures of native bacteriorhodopsin depend on the molecular packing arrangement in the membrane. *J. Mol. Biol.* 285:1903–1909.
19. Garcia-Manyes, S., and F. Sanz. 2010. Nanomechanics of lipid bilayers by force spectroscopy with AFM: a perspective. *Biochim. Biophys. Acta.* 1798:741–749.
20. Sullan, R. M. A., J. K. Li, and S. Zou. 2009. Direct correlation of structures and nanomechanical properties of multicomponent lipid bilayers. *Langmuir.* 25:7471–7477.
21. Sullan, R. M. A., J. K. Li, …, S. Zou. 2010. Cholesterol-dependent nanomechanical stability of phase-segregated multicomponent lipid bilayers. *Biophys. J.* 99:507–516.
22. Garcia-Manyes, S., G. Oncins, and F. Sanz. 2005. Effect of ion-binding and chemical phospholipid structure on the nanomechanics of lipid bilayers studied by force spectroscopy. *Biophys. J.* 89:1812–1826.
23. Garcia-Manyes, S., G. Oncins, and F. Sanz. 2005. Effect of temperature on the nanomechanics of lipid bilayers studied by force spectroscopy. *Biophys. J.* 89:4261–4274.
24. Ly, H., D. Block, and M. Longo. 2002. Interfacial tension effect of ethanol on lipid bilayer rigidity, stability, and area/molecule: a micropipette aspiration approach. *Langmuir.* 18:8988–8995.
25. Leonenko, Z. V., A. Carnini, and D. T. Cramb. 2000. Supported planar bilayer formation by vesicle fusion: the interaction of phospholipid vesicles with surfaces and the effect of gramicidin on bilayer properties using atomic force microscopy. *Biochim. Biophys. Acta.* 1509: 131–147.
26. Sader, J. E., I. Larson, …, L. R. White. 1995. Method for the calibration of atomic force microscope cantilevers. *Rev. Sci. Instrum.* 66:3789–3798.
27. Pirzer, T., and T. Hugel. 2009. Atomic force microscopy spring constant determination in viscous liquids. *Rev. Sci. Instrum.* 80:035110-1–035110-6.
28. Charitat, T., E. Bellet-Amalric, …, F. Graner. 1999. Adsorbed and free lipid bilayers at the solid-liquid interface. *Eur. Phys. J. B.* 8:583–593.
29. Kim, J., G. Kim, and P. S. Cremer. 2001. Investigations of water structure at the solid/liquid interface in the presence of supported lipid bilayers by vibrational sum frequency spectroscopy. *Langmuir.* 17:7255–7260.
30. Cremer, P., and S. Boxer. 1999. Formation and spreading of lipid bilayers on planar glass supports. *J. Phys. Chem. B.* 103:2554–2559.
31. Dimitriadis, E. K., F. Horkay, …, R. S. Chadwick. 2002. Determination of elastic moduli of thin layers of soft material using the atomic force microscope. *Biophys. J.* 82:2798–2810.
32. Hertz, H. 1881. On the contact of solid elastic bodies. *J. reine und angewandte Mathematik.* 92:156–171.
33. Fukuma, T., M. J. Higgins, and S. P. Jarvis. 2007. Direct imaging of individual intrinsic hydration layers on lipid bilayers at Angstrom resolution. *Biophys. J.* 92:3603–3609.
34. Landau, L. D., E. M. Lifshitz, …, P. L. Pitaevskii. 1986. Theory of Elasticity, 3rd ed. Butterworth-Heinemann.

35. Rawicz, W., K. C. Olbrich, …, E. Evans. 2000. Effect of chain length and unsaturation on elasticity of lipid bilayers. *Biophys. J.* 79:328–339.

36. Li, S., F. Eghiaian, …, I. A. Schaap. 2011. Bending and puncturing the influenza lipid envelope. *Biophys. J.* 100:637–645.

37. Smeulders, J. B., C. Blom, and J. Mellema. 1990. Linear viscoelastic study of lipid vesicle dispersions: hard-sphere behavior and bilayer surface dynamics. *Phys. Rev. A.* 42:3483–3498.

38. Marquês, J. T., A. S. Viana, and R. F. M. De Almeida. 2011. Ethanol effects on binary and ternary supported lipid bilayers with gel/fluid domains and lipid rafts. *Biochim. Biophys. Acta.* 1808:405–414.

39. Picas, L., F. Rico, and S. Scheuring. 2012. Direct measurement of the mechanical properties of lipid phases in supported bilayers. *Biophys. J.* 102:L01–L03.

40. Klemm, W. R. 1998. Biological water and its role in the effects of alcohol. *Alcohol.* 15:249–267.

41. Separovic, F., and K. Gawrisch. 1996. Effect of unsaturation on the chain order of phosphatidylcholines in a dioleoylphosphatidylethanolamine matrix. *Biophys. J.* 71:274–282.

42. Yoon, R. H., and S. Vivek. 1998. Effects of short-chain alcohols and pyridine on the hydration forces between silica surfaces. *J. Colloid Interface Sci.* 204:179–186.